TAILORING OF CONTINUOUS CARBON FIBER REINFORCED POLYMER LATTICE STRUCTURES

N. Ichihara[1], M. Ueda[2]

[1] Nihon University, 1-8-14 Kanda Surugadai, Chiyoda, Tokyo, Japan, ichihara.naruki@nihon-u.ac.jp
[2] Nihon University, 1-8-14 Kanda Surugadai, Chiyoda, Tokyo, Japan, masahito.ueda@nihon-u.ac.jp

Keywords: 3D printing, Optimization, Continuous carbon fibre, Lattice

ABSTRACT

The high-stiffness 3D-printed continuous carbon fiber reinforced polymer composite structure was proposed based on concurrent topology and material orientation optimization. The multi-variable topology optimization was performed with the Cartesian representation of orientation. The 3D print path was developed from the optimized result by means of the stripe pattern method. To reduce the number of fiber-cutting processes due to discontinuous paths, a modified travel salesman problem was adopted.

1 INTRODUCTION

Topology optimization provides optimal material distribution that minimizes material usage with high stiffness. The topology-optimized structures have complex geometry that is difficult to build with conventional manufacturing processes. Additive manufacturing technologies enable the fabrication of these complex structures. In recent developments in additive manufacturing, continuous carbon fiber reinforced polymer (CFRP) composites are also 3D-printable [1]. However, topology-optimized complex structures have holes and branches that cause fiber discontinuity and limit mechanical performance. The material orientation and its continuity are essential as well as the external shape design for the CFRP structures.

The material properties vary everywhere in the optimized CFRP structure. Free Material Optimization (FMO) method provides the highest degree of freedom of the design space, which results in the numerically best structure [2]. However, the optimized material properties vary everywhere in the structure, and it is often difficult to fabricate. Discrete Material Optimization (DMO) method assumes a finite number of material properties and optimizes the weight vector that selects the material properties [3]. For example, four directions of material orientation i.e., 0°, 45°, 90°, and 135° are selected and optimized for CFRP. However, in the 3D printing of CFRP, the material orientation changes arbitrary because the curvilinear printing path is enabled. Continuous Fiber Angle Optimization (CFAO) method provides both optimized material distribution and the material angle using an Eulerian angle representation [4]. However, optimization of the Eulerian angle becomes a local optimum problem due to the non-convex design space. The Cartesian vector representation of material angle overcomes this problem [5]. The print path needs to be continuous for continuous carbon fiber printing although the discretised material angle is obtained by the optimization. The de-homogenization approach is needed to generate a continuous print path that follows the discretised material angle field. The stripe pattern projection-based approach is suitable to generate optimized print paths from the discretised material angle field [7].

This study investigated the numerical optimization scheme for the high-stiffness continuous carbon fiber-reinforced polymer lattice structures. The scheme was based on the homogenized multi-field optimization method with Cartesian orientation representation. The stripe pattern-based de-homogenization method was adopted to generate the continuous 3D printing path from the discretized material angle field obtained by the optimization. The print paths were arranged by solving the modified travel salesman problem to minimize the number of fiber-cutting process.

2 OPTIMIZATION FORMULATION

2.1 Design variables

The design domain D is given, and the topology variable χ was defined as follows:

$$\chi(\mathbf{x}) = \begin{cases} 1 & \text{for } \forall \mathbf{x} \in \Omega \\ 0 & \text{for } \forall \mathbf{x} \in D \backslash \Omega \end{cases} \tag{1}$$

where $\mathbf{x}$ is the position vector on the design domain D, Ω represents the material region, and $D\backslash\Omega$ indicates the void region. This topology variable leads to the ill-posed problem because of its discontinuity in the design space. The hyperbolic tangent-based Heaviside filter was adopted to relax the topology variable of Eq. (1) as follows:

$$\tilde{\chi}(\mathbf{x}) = H\big(\phi(\mathbf{x})\big) = \frac{\tanh \beta\eta + \tanh \beta(\phi(\mathbf{x}) - \eta)}{\tanh \beta\eta + \tanh \beta(1 - \eta)} \tag{2}$$

where β, η are constants. $\phi(\mathbf{x})$ is defined as the precursor variable for the topology.

The material orientation was defined with Cartesian representation:

$$\boldsymbol{\theta}(\mathbf{x}) = \begin{bmatrix} \theta_1 \\ \theta_2 \end{bmatrix}. \tag{3}$$

This vector should be unity,

$$\|\boldsymbol{\theta}\| = 1. \tag{4}$$

However, these constraints cause the discontinuity of design space and lead the non-convex ill-posed optimization. Here the constraint was relaxed as

$$\|\boldsymbol{\theta}\| \leq 1. \tag{5}$$

This relaxation was similar to the Heaviside projection of the topology variable (Eq. (2)). The constraint of Eq. (5) is the position-wised constraint. The isoparametric projection method was adopted to reduce the constraint of optimization. The isoparametric projection projects a vector on the natural coordinate system to the Cartesian coordinate system:

$$N: \mathcal{N} \to \mathcal{R}, \mathcal{N} = \{\, \boldsymbol{a} \mid \forall \boldsymbol{a} \in [-1,1]^2 \} \to \mathcal{R} = \{\, \boldsymbol{b} \mid \forall \boldsymbol{b} \in \|\boldsymbol{b}\| \leq 1 \} \tag{6}$$

The precursor vector variable for orientation $\boldsymbol{\vartheta}$ was proposed and the orientation vector was represented as follows:

$$\boldsymbol{\theta}(\mathbf{x}) = N\big(\boldsymbol{\vartheta}(\mathbf{x})\big). \tag{7}$$

The isoparametric projection was detailed in Ref. [5].

An additional design variable i.e., material density variable ρ is introduced. This variable is the independent variable of topology. The material density variable ρ varies the stiffness tensor $\mathbb{C}^{\rho}(\rho)$ that was associated with the lattice configurations. In this study, the material density of the lattice was controlled by the hatch spacing of the print path. The relationship of $\mathbb{C}^{\rho}$ and ρ was obtained by the asymptotic homogenization, as discussed in the following. The material density variable was defined as follows:

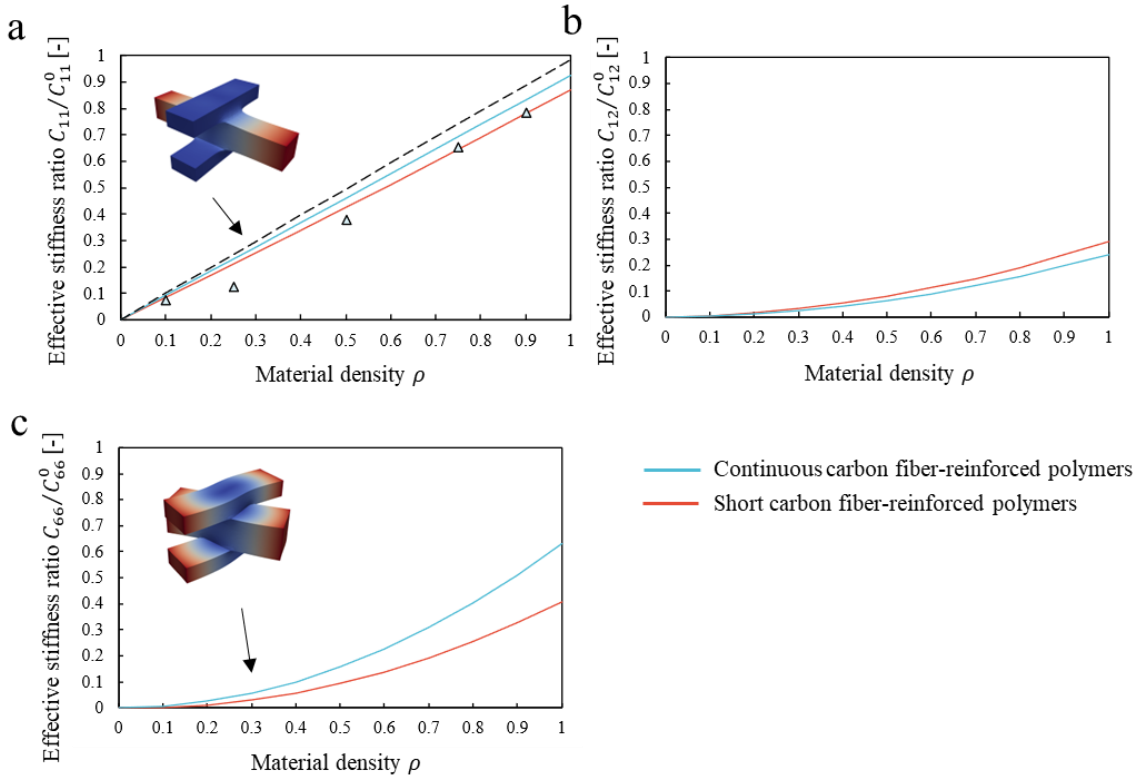

Figure 1: Relationship between the material density and effective stiffness ratios.

$$\rho(\mathbf{x}) \in [\rho_{min}, \rho_{max}]. \tag{8}$$

where ρ_{min}, ρ_{max} represent the lower and upper bounds of material density.

2.2 Material representation

This subsection represents the material constitutive equations associated with the above design variables. The relationship between the stiffness tensor $\mathbb{C}^{\rho}$ and the material density ρ was calculated by asymptotic homogenization. Here, the symmetric cross-plied lattice configuration was assumed, as illustrated in Fig. 1. The material density was varied with the hatch spacing between paths. The orthotropic properties directed to the print paths were used because the modulus is maximum in the printing direction and minimum in the transverse direction. The homogenized lattice properties exhibit the same modulus for the two orthogonal directions because of the cross-plied configuration. Thus, the number of independent elements of the stiffness tensor was three, $C_{11}(= C_{22})$, C_{12}, and C_{66}. The normalized components of stiffness tensor obtained by the asymptotic homogenization were plotted in Fig. 1.

The reduced stiffness tensor $\mathbb{C}^{\rho}(\rho)$ was rotated by the orientation vector $\boldsymbol{\theta}$. Here, the rotation tensor $T(\boldsymbol{\theta})$ was defined, and the rotated stiffness tensor $\mathbb{C}^{\boldsymbol{\theta}}$ was represented as follows:

$$\mathbb{C}^{\boldsymbol{\theta}}(\rho, \boldsymbol{\theta}) = T^{-1}(\boldsymbol{\theta})\mathbb{C}^{\rho}(\rho)T(\boldsymbol{\theta}), \tag{9}$$

where T^{-1} represents the inverse tensor of the rotation tensor.

The topology variable was inserted into the stiffness tensor that defined the optimized external design. Here the penalization approach was used, and the stiffness tensor was defined as follows:

$$\mathbb{C}(\rho, \boldsymbol{\theta}, \chi) = \mathbb{C}_{void} + \tilde{\chi}^{p}\left(\mathbb{C}^{\boldsymbol{\theta}}(\rho, \boldsymbol{\theta}) - \mathbb{C}_{void}\right). \tag{10}$$

where $p = 3$ is the penalty and $\mathbb{C}_{void}$ is the void tensor that was set to be a small value.

2.3 Regularization of design variables

The regularization of the design vector was conducted to make the optimization process a well-posed problem. The regularization was based on a partial differential equation type filter, Helmholtz filtering. All (precursor) design variables were vectorized as a single design vector:

$$\boldsymbol{d} = \begin{bmatrix} \rho \\ \boldsymbol{\vartheta} \\ \phi \end{bmatrix}, d \in \left[\rho_{min}, \rho_{max}\right] \times [-1,1]^2 \times [0,1]. \tag{11}$$

Then, the Helmholtz equation was defined as follows:

$$-R^2\nabla^2\boldsymbol{d} + \boldsymbol{d} = \boldsymbol{d} \tag{12}$$

where R is the filter radius and $\boldsymbol{d}$ is the filtered design vector.

2.4 Compliance minimization problem

A compliance minimization problem is selected in this study. The problem is defined as follows:

$$\min_{\boldsymbol{d}} F = \int_D \boldsymbol{\varepsilon} : \mathbb{C}(\rho, \boldsymbol{\theta}, \chi) : \boldsymbol{\varepsilon} \ \mathrm{d}\Omega. \tag{13a}$$

Subject to:

$$\boldsymbol{\varepsilon} = \frac{1}{2}(\nabla\boldsymbol{u} + \nabla\boldsymbol{u}^T) \tag{13b}$$

$$\nabla \cdot (\boldsymbol{\varepsilon} \cdot \mathbb{C}) = 0 \text{ in } D, \boldsymbol{u} = 0 \text{ on } \Gamma_D, \nabla \cdot (\boldsymbol{\varepsilon} \cdot \mathbb{C}) \cdot \boldsymbol{n} = \boldsymbol{t} \text{ on } \Gamma_N \tag{13c}$$

$$g(\boldsymbol{d}) = \int_D \tilde{\chi}\rho \ \mathrm{d}\Omega - \bar{V} \leq 0 \tag{13d}$$

where $\boldsymbol{\varepsilon}$ and $\boldsymbol{u}$ are strain tensor and displacement vector, respectively. Γ_D and Γ_N are Dirichlet and Neumann boundaries. $\boldsymbol{t}$ and $\boldsymbol{n}$ represent the traction vector and the normal vector, respectively. $\bar{V}$ is the volume fraction of the whole structure. The displacement vector $\boldsymbol{u}$ was discretized on the first-order triangle Lagrange element space. The design vector $\boldsymbol{d}$ was also defined on the same element space. The finite element method (FEM) was conducted to resolve the elastic equilibrium. The FEM was performed in Python 3.11 with the FEniCS 2019, a FEM package based on PETSc. The method of moving asymptotes that was built in the NLopt package updated the design vector iteratively.

3 TOOL-PATH GENERATION

This subsection represents the generation of continuously varied stripe pattern that follows the optimized design vector $\boldsymbol{d}$. The stripe pattern projection approach was adopted. The i-th parameterization φ_i drived the stripe pattern Φ_i such as cosine projection:

$$\Phi_i = \cos p\varphi_i \tag{14}$$

where wavelength p was related to the material density ρ and topology χ:

$$p = \frac{\pi\rho\chi}{w_0} \tag{15}$$

where w_0 is print path width. The parameterization φ_i was defined based on the optimized material orientation $\boldsymbol{\theta}_i$. The parameterization φ_i was computed by minimizing the following latest-squares error:

$$\min_{\varphi_i} \Psi = \int_D \left| \nabla \varphi_i - \boldsymbol{\theta}_i^{\perp} \right|^2 \mathrm{d}\Omega . \tag{16}$$

$\boldsymbol{\theta}_i$ is the i-th layer of the orientation field that was cross-plied sequence as follows:

$$\boldsymbol{\theta}_i = [\angle\boldsymbol{\theta}/\angle\boldsymbol{\theta} + 90° = \boldsymbol{\theta}^{\perp}]_{(N/2)S} \tag{17}$$

N and S are the numbers of total layers and symmetric symbols, respectively. To obtain the lattice structure, Eq. (17) needs to be resolved with two vector fields, $\boldsymbol{\theta}_i^{\perp}$ and $\boldsymbol{\theta}_i$.

The print paths $\mathcal{C}_j$ on j-th layer are extracted from a contour line of the stripe pattern. The paths $\mathcal{C}_j$ were arranged to reduce the number of fiber-cutting processes. In this study, a modified travel salesman problem with a greedy solver was conducted. Each path has a start node $\boldsymbol{x}_j^S$ and end node $\boldsymbol{x}_j^E$. The identical number was labeled to all nodes as:

$$\boldsymbol{x} = \left\{ \boldsymbol{x}_1^S, \boldsymbol{x}_2^S, \dots, \boldsymbol{x}_j^S, \dots, \boldsymbol{x}_M^S, \boldsymbol{x}_{M+1}^E, \boldsymbol{x}_{M+2}^E, \dots, \boldsymbol{x}_{M+j}^E, \dots, \boldsymbol{x}_{2M}^E \right\} \tag{18}$$

where M represents the total number of paths. The distance matrix $\mathbb{D}$ was calculated based on the above node vector. However, the nodes between the start and end points of each path should be connected. The modified distance matrix $\widehat{\mathbb{D}}$ was defined with the following distance function $\hat{d}_{kl}$:

$$\widehat{\mathbb{D}} = \hat{d}_{kl} = \begin{cases} \|\boldsymbol{x}_k - \boldsymbol{x}_l\| & \text{if } l - M \neq k \\ 0 & \text{if } l - M = k \end{cases} \tag{19}$$

The connecting path information was embedded into the modified distance matrix $\widehat{\mathbb{D}}$. The greedy solver was adopted to solve the travel salesman problem.

4 OPTIMIZED STRUCTURES

The proposed optimization framework was applied to a two-dimensional bracket problem as shown in Fig. 2(a). The bracket has three holes where deformation is constrained at a hole and loads are applied at the other holes. The weight reduction rate was set to be 50% and the upper and lower bounds of the material density variable were $\rho_{min} = 0.5, \rho_{max} = 1.0$, respectively. Fig. 2(b) represents the optimized material direction and material density. Fig. 2(c) shows the obtained print path based on the optimized result in Fig. 2(b).

5 CONCLUSIONS

This study proposed the concurrent optimization of the material orientation and distribution for the 3D-printed continuous carbon fiber reinforced polymer composite lattice structures. The multi-variable topology optimization based on Cartesian orientation and Helmholtz filter was conducted. The Helmholtz filter improved the continuity of the material orientation field. The stripe pattern projection approach was used to generate the 3D print paths that aligned to the optimized material orientation. The modified travel salesman problem was adopted to reduce the fiber-cutting process by arranging the print path. The method was applied to a two-dimensional bracket problem. Optimized print path was obtained based on the optimized result of the material orientation and material density.

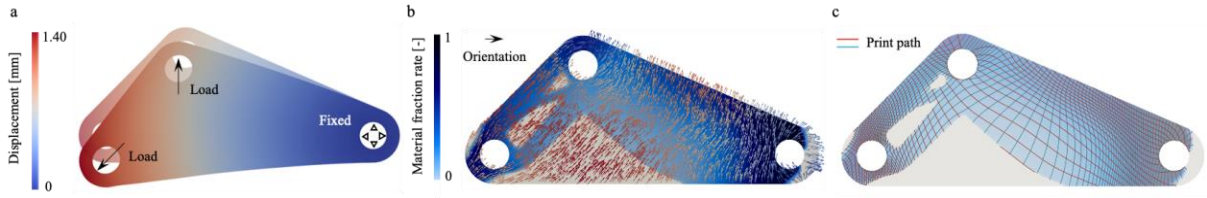

Figure 2: Optimized 3D print path for 3-hole and multi-loading bracket example. (a) The geometrical setting and boundary conditions. The color map shows displacement magnitude. (b) Optimized material distribution and orientation. (c) Print path conformed optimization result.

REFERENCES

[1] P. Cheng, Y. Peng, S. Li, Y. Rao, A. Le Duigou, K. Wang and S. Ahzi, 3D printed continuous fiber reinforced composite lightweight structures: A review and outlook, *Composites Part B: Engineering*, 250, 2023, 110450 (https://doi.org/10.1016/j.compositesb.2022.110450).

[2] J. Zowe, M. Kočvara, and M.P. Bendsøe, Free material optimization via mathematical programming, *Mathematical Programming*, 79, 1997, pp. 445-466 (https://doi.org/10.1007/BF02614328).

[3] J. Stegmann and E. Lund, Discrete material optimization of general composite shell structures, *International Journal for Numerical Methods in Engineering*, 62, 2005, pp. 2009-2027 (https://doi.org/10.1002/nme.1259).

[4] D. Jiang, R. Hoglund, and D.E. Smith, Continuous Fiber Angle Topology Optimization for Polymer Composite Deposition Additive Manufacturing Applications, *Fibers*, 7, 2019, (https://doi.org/10.3390/fib7020014)

[5] T. Nomura, E. M. Dede, J. Lee, S. Yamasaki, T. Matsumori, A. Kawamoto and N. Kikuchi, General topology optimization method with continuous and discrete orientation design using isoparametric projection, *International Journal for Numerical Methods in Engineering*, 101, 2015, pp. 571-605, (https://doi.org/10.1002/nme.4799).

[6] Z. Yang, K. Fu, Z. Zhang, J. Zhang and Y. Li, Topology optimization of 3D-printed continuous fiber-reinforced composites considering manufacturability, *Composites Science and Technology*, 230, 2022, 109727, (https://doi.org/10.1016/j.compscitech.2022.109727)

[7] N. Ichihara and M. Ueda, 3D-printed high-toughness composite structures by anisotropic topology optimization, *Composites Part B: Engineering*, 253, 2023, 220572 (https://doi.org/10.1016/j.compositesb.2023.110572).